LOWER BOUND FOR ELECTRON CORE BETA IN THE SOLAR WIND

S. Peter Gary
Los Alamos National Laboratory
Los Alamos, NM 87545

Jennifer A. Newbury
University of California
Los Angeles, CA 90095

Bruce E. Goldstein
Jet Propulsion Laboratory
Pasadena, CA 91109

10 March 1998

Abstract

Solar wind electrons, especially under conditions of relatively low speed flow, often can be represented as two bi-Maxwellian components, a cooler more dense core (denoted by the subscript c) and a hotter more tenuous halo. Solar wind observations from Ulysses between 1.5 and 2 AU further indicate that the β for electron core temperatures parallel to the background magnetic field, $\beta_{\|c}$, has a distinct lower bound near 0.1. To seek the cause of this possible constraint, this manuscript uses numerical solutions of the full Vlasov linear dispersion equation for four heat flux instabilities under a core/halo model with parameters representative of the solar wind near 1 AU. In this model the whistler heat flux instability is the growing mode of lowest threshold at most observed values of $\beta_{\|c}$. As $\beta_{\|c}$ is decreased, however, the growth of this mode is reduced, so that at sufficiently small values of this parameter the Alfvén heat flux instability or the electron/ion acoustic instability becomes the fastest growing mode. The critical condition corresponding to this transition is calculated as a function of $T_{\|c}/T_p$ (where T_p is the proton temperature) and approximately corresponds to the observed constraint at $\beta_{\|c} \simeq 0.1$. The Alfvén and ion acoustic instabilities both resonate with core electrons; this manuscript proposes the hypothesis that core heating by these two modes at the critical condition establishes a lower bound on $\beta_{\|c}$.

Introduction

Newbury et al. [1998] analyzed data from solar wind spacecraft ISEE-3 and Ulysses to demonstrate that there is a clear lower bound in the electron temperature T_e as plotted versus the proton temperature T_p, corresponding to the condition

$$T_e = \tau_{ep} T_p + T_{eo} \tag{1}$$

where τ_{ep} and T_{eo} are fitting parameters which change with solar wind conditions. Their analysis of ISEE-3 data from near 1 AU indicates an overall lower bound at $T_{eo} \simeq 4$ eV, but a slope of Equation (1), τ_{ep}, ranging from 0.47 for slow speed solar wind to 0.23 for the high speed wind. Data analysis from ISEE-3 by *Richardson et al.* [1997] indicates $\tau_{ep} \simeq 1$ in plasmas of coronal mass ejections.

If the constraint represented by Equation (1) is imposed by small-scale processes in the collisionless solar wind, those processes should be described by the Vlasov equation. Because solutions to the Vlasov equation can be completely expressed in terms of dimensionless variables, such variables should be used in searches for the consequences of plasma microprocesses. For purposes of illustration, let us assume that the electron density n_e and the magnitude of the background magnetic field $\mathbf{B}_o$ have much smaller variations than T_e. Then Equation (1) can be written

$$\frac{T_e}{T_p} = \frac{\tau_{ep}}{\left(1 - \frac{\beta_{eo}}{\beta_e}\right)} \tag{2}$$

which represents two lower bounds:

$$\beta_e \geq \beta_{eo} \tag{3}$$

and

$$\frac{T_e}{T_p} \geq \tau_{ep} \tag{4}$$

where $\beta_e \equiv 8\pi n_e k_B T_e / B_o^2$ and where β_{eo} corresponds to T_{eo}, the intercept of Equation (1).

The data analyses of *Newbury et al.* [1998] and *Richardson et al.* [1997] considered only an overall electron temperature. However, in the undisturbed low latitude solar wind near 1 AU at flow speeds of about 500 km/sec or less, the electron velocity distribution is frequently well represented as two components, a more dense, cooler core (denoted by subscript c) and a hotter, more tenuous halo (subscript h) [*Feldman et al.*, 1975]. Each of

these components is approximately described by a bi-Maxwellian distribution; the average velocities of each component are such that there is zero net charge and zero net current but there is a net heat flux q_e pointing along $\mathbf{B}_o$ and away from the sun. Similarly, in the low speed solar wind the proton distribution is typically observed to be Maxwellian-like. In contrast, at higher flow speeds a third electron component, the "strahl," appears, and proton beams frequently arise [*Feldman et al.*, 1974; *Marsch*, 1991]. The analyses, both theoretical and observational, presented here are based on the core/halo electron and single Maxwellian proton model distribution models of the slow speed wind. In this model the dimensionless parameters which characterize the densities and thermal properties of the solar wind electron components are $\tilde{\beta}_{\|c}$, n_h/n_e, $T_{\|h}/T_{\|c}$, $T_{\perp h}/T_{\|h}$, $T_{\perp c}/T_{\|c}$, and q_e/q_{max} (See the Appendix for definitions of the various quantities and symbols.).

To test the possibility that solar wind observations may exhibit constraints on dimensionless, as well as dimensional, parameters, we examined data from the Ulysses mission, using observations made with the Los Alamos solar wind ion and electron SWOOPS spectrometers [*Bame et al.*, 1992]. Specifically, we considered data gathered during January 1991, when Ulysses travelled from 1.59 AU to 1.93 AU in the ecliptic plane. During this month, the solar wind flow speed was observed to range between 290 and 445 km/s; in other words, no high speed streams were observed.

We used the Ulysses three-dimensional electron data set, utilizing parameters derived from bi-Maxwellian fits to both the core and halo velocity distributions. This data set includes the corrections for spacecraft potential developed and described by *Scime et al.* [1994a]. Even with such corrections, we found some intervals during which the total electron and proton densities were significantly different; the likely sources of this discrepancy are the difficulty in distinguishing between photoelectrons from the spacecraft and core electrons of similarly low energy and the associated problem of accurately determining the spacecraft potential. To exclude data with large density differences, we included only points meeting the criterion $|n_e - n_p|/n_p < 0.5$. Application of this criterion excluded 12% of the 779 points which constitute the three-dimensional data set for January 1991.

Scime et al. [1994a] has demonstrated that the SWOOPS instrument can measure accurately electron core densities as small as 0.02 cm^{-3}, and *Maksimovic et al.* [1995] has shown that the same instrument can determine electron core temperatures accurately down to at least 4 eV. With these values, $\tilde{\beta}_{\|c} \leq 0.1$ corresponds to $B_o \geq 2$ nT, which values are routinely measured by the Ulysses magnetometer. Therefore, Ulysses instrumentation

is fully capable of measuring relatively low values of the core β. However, from our 685 data points we found only a single point which satisfied $\tilde{\beta}_{\|c} \leq 0.1$. This is illustrated in Figure 1 which plots the halo temperature anisotropy as a function of the core parallel β. The $T_{\perp h}/T_{\|h}$ is plotted here as a representative dimensionless parameter; plots of other such parameters would show the same $\tilde{\beta}_{\|c}$ distribution. This absence of observations at low values of this parameter resembles a similar absence of observations of large $T_{\perp p}/T_{\|p}$ values in both the magnetosheath [*Anderson and Fuselier*, 1993; *Anderson et al.*, 1994; *Fuselier et al.*, 1994] and the outer magnetosphere [*Gary et al.*, 1995]. This latter effect has been explained as an upper bound on the proton temperature anisotropy which is imposed by wave-particle scattering by the electromagnetic proton cyclotron anisotropy instability [*Gary et al.*, 1994a]. To determine whether another wave-particle effect is bounding $\tilde{\beta}_{\|c}$ in the solar wind, we here consider heat flux instabilities as potential sources of electron heating when $\tilde{\beta}_{\|c}$ becomes sufficiently small.

An electron heat flux in a plasma corresponds to an anisotropy of the electron velocity distribution and, as such, bears free energy, that is, the capability to drive relatively short wavelength microinstabilities. Such instabilities lead to the growth of enhanced short wavelength field fluctuations; these fluctuations scatter plasma particles, acting to reduce the driving anisotropy and thereby limiting q_e. If we consider a sufficiently broad domain of parameters, there are several different such instabilities which may grow in the solar wind; in the core/halo model there are at least the whistler, magnetosonic, and Alfvén heat flux and electron/ion acoustic instabilities [*Gary*, 1993]. Each of these growing modes has its own peculiar dispersion properties and its own distinguishing wave-particle interactions; in each case the enhanced fluctuations act to limit the heat flux in a different way. So although each instability may impose an upper bound on q_e, each also may provide constraints on other plasma parameters at the same time.

Assumptions and Procedure

We begin with two general assumptions. Our first is that the constraints on dimensionless plasma parameters observed in the solar wind are due to the action of microinstabilities; that is, relatively short wavelength ($ka_p \gtrsim 0.1$ where k is the wavenumber and a_p is the proton gyroradius) growing modes in the plasma which lead to enhanced fluctuations which, in turn, scatter the electrons and ions. Our second assumption is that such constraints correspond to the threshold conditions of one or more microinstabilities.

We then make a series of more specific assumptions which underlie the detailed calculations to follow. We assume that, among the many different types of anisotropies which may excite microinstabilities in the solar wind, the heat flux carried by the electrons is the primary source of free energy for growth of field fluctuations which determine the constraint of interest here. We assume that the core/halo description established by *Feldman et al.* [1975] is an appropriate model for electrons in the low speed solar wind. Further we assume that the relative core/halo average drift speed v_o can vary rapidly so that the associated electron heat flux also exhibits relatively fast, relatively large fluctuations.

Then from the first assumption it follows that constraints such as Equation (3) and Equation (4) are due to electron heating, because the wave-particle scattering due to such instabilities is a stochastic process which leads to an increase rather than a decrease of any species temperature. The last assumption above implies that, on a fast time scale, the heat flux will become large enough to locally excite the fastest growing mode; this in turn implies that the maximum growth rate is an appropriate quantity to measure the efficacy of the various instabilities.

Using all these assumptions, we have studied how the maximum growth rates of various heat flux instabilities respond to gradual changes in the core parallel β, specifically seeking transitions from conditions favoring the growth of one instability to conditions more favorable for growth of another mode. We have found such a transition, quantified it and compared it against solar wind observations to show that such a transition corresponds to the observed constraint.

Heat Flux Instabilities: Linear Theory

We use the *Feldman et al.* [1975] model of bi-Maxwellian distributions to model both the core and halo electron components. We ignore heavy ions and assume that the solar wind protons may be represented as a single isotropic Maxwellian velocity distribution, so that $T_{\|p} = T_{\perp p} = T_p$ and proton thermal properties are represented by a single dimensionless parameter, $T_{\|c}/T_p$. We assume quasineutrality, so that $n_e = n_c + n_h = n_p$. Table 1 presents the dimensionless parameter values used in *Gary et al.* [1975, 1994b]; unless otherwise stated, these are the parameters used throughout our linear calculations. Except for the core and halo temperature anisotropies [e.g., *Phillips et al.*, 1995], these parameters represent average solar wind parameters near 1 AU. Because average dimensionless parameters vary relatively weakly with distance from the sun [e.g., Table 2 of *Gary et al.*, 1994b], our theoretical results derived from the parameters of Table 1 should also

Table 1. Parameter model from Gary et al. [1975]

Parameter	Protons	Core Electrons	Halo Electrons
m_j/m_p	1.0	1/1836	1/1836
e_j/e_p	1.0	-1.0	-1.0
n_j/n_e	1.0	$1 - n_h/n_e$	0.05
$T_{\|j}/T_p$	1.0	2.0	12.0
$T_{\perp j}/T_{\|j}$	1.0	1.0	1.0

$$v_A/c = 1 \times 10^{-4}$$

be approximately valid for our comparison against the Ulysses data set gathered from 1.59 AU to 1.93 AU.

We first consider the three electromagnetic growing modes which *Gary et al.* [1975a, b] identified as the most likely to be excited by an electron heat flux near 1 AU: the whistler, the magnetosonic, and the Alfvén heat flux instabilities.

The whistler heat flux instability is a relatively high frequency ($\omega_r >> \Omega_p$), short wavelength ($kc/\omega_p >> 1$) mode with maximum growth rate at $\mathbf{k} \times \mathbf{B}_o = 0$ and which propagates in the direction of the heat flux (i.e. ω_r and v_{oh} have the same sign). Representative dispersion properties of this mode are illustrated in Fig. 8.8 of *Gary* [1993]; the dispersion properties of the instability correspond to a cyclotron resonant halo ($2 \lesssim |\zeta_h^+| \lesssim 3$), a weakly resonant core ($4 \lesssim |\zeta_c^+|$) and nonresonant protons ($1 << |\zeta_p^+|$).

The nonresonant character of the protons implies that the properties of the whistler heat flux instability are essentially independent of variations in $T_{\|c}/T_p$ and β_p if all dimensionless parameters involving only electron properties are held constant. Numerical solutions of the linear Vlasov equation dispersion equation show that this is indeed true. On the other hand, the resonant properties of the halo suggest that the properties of this instability vary strongly with the dimensionless parameters $T_{\|h}/T_{\|c}$, $T_{\perp h}/T_{\|h}$, and $\tilde{\beta}_{\|c}$.

The Alfvén heat flux instability [e.g., *Forslund*, 1970] propagates at $\omega_r < \Omega_p$, $kc/\omega_p < 1$ and with $\mathbf{k}$ at a relatively large angle ($\theta \sim 80^o$) relative to $\mathbf{B}_o$. A representative dispersion plot is illustrated in Fig. 1 of *Gary et al.* [1975a]. The oblique character of this instability implies that it can sustain both Landau and cyclotron resonances. Representative solutions of the linear Vlasov dispersion equation for this mode yield $|\zeta_p| \gtrsim 3$, $|\zeta_p^-| \sim 3$, and $|\zeta_p^+| >> 1$; $0 < |\zeta_c| << 1$ and $|\zeta_c^\pm| >> 1$; as well as $|\zeta_h| \sim 1$ and $|\zeta_h^\pm| >> 1$. Thus the strongest

wave-particle interaction of the Alfvén heat flux instability is the Landau resonance with the electron core.

The magnetosonic heat flux instability [e.g., *Forslund*, 1970] propagates at $\omega_r < \Omega_p$, $kc/\omega_p < 1$ and with $\mathbf{k}$ at an intermediate angle ($30^o \lesssim \theta \lesssim 50^o$) relative to $\mathbf{B}_o$. Representative dispersion plots of this growing mode are illustrated in Fig. 2 of *Gary et al.* [1975a]. Solutions of the linear Vlasov dispersion equation for this mode typically yield $|\zeta_p| >> 1$, $|\zeta_p^-| \sim 3$, and $|\zeta_p^+| >> 1$; $0 < |\zeta_c| << 1$ and $|\zeta_c^\pm| >> 1$; as well as $|\zeta_h| \sim 0.5$ and $|\zeta_h^\pm| >> 1$.

Fig. 3 of *Gary et al.* [1975b] compares the threshold conditions of these three modes, showing that the whistler heat flux instability has the lowest threshold among the three for representative conditions at 1 AU, $0.10 < \beta_p \leq 1.0$ and $1 \leq T_{\|c}/T_p \leq 4$. This result suggests that the whistler is an important mechanism for the limitation of the heat flux in the solar wind near 1 AU, and has led to several detailed studies of this mode [e.g., *Gary and Feldman*, 1977; *Dum et al.*, 1980; *Gary et al.*, 1994b]. However, our concern here is with relatively low values of core electron β, so it is necessary to compare the properties of the three electromagnetic heat flux instabilities over a broader range of $T_{\|c}/T_p$ values and $\tilde{\beta}_{\|c} \leq 0.10$.

Figure 2 compares the maximum growth rates of these three growing modes as a function of the dimensionless electron heat flux for three different values of $\tilde{\beta}_{\|c}$ with all other dimensionless variables as given in Table 1. At $\tilde{\beta}_{\|c} \gtrsim 0.2$, the whistler instability is clearly the dominant growing mode with both the lowest threshold value of the dimensionless heat flux and the fastest growth rate. As $\tilde{\beta}_{\|c}$ is decreased, however, this instability becomes less important: its threshold value of q_e/q_{max} increases, the γ_m/Ω_p for a given dimensionless heat flux decreases, and the overall maximum growth rate for all values of q_e/q_{max} also decreases. For these parameters the magnetosonic heat flux instability is not competitive; both γ_m/Ω_p and γ_{mm}/Ω_p generally decrease with a decrease in $\tilde{\beta}_{\|c}$. The Alfvén heat flux instability also suffers an increasing threshold and decreasing γ_m/Ω_p with decreasing core parallel β. However, the Alfvén mode does not exhibit an overall maximum growth rate γ_{mm}; rather, for the domain of q_e/q_{max} considered here, γ_m/Ω_p increases monotonically with increasing heat flux. So at sufficiently small $\tilde{\beta}_{\|c}$, the Alfvén heat flux instability becomes the dominant mode in the sense that it attains the lowest heat flux threshold as well as the largest overall growth rate.

A fourth mode which can be unstable in the core/halo model of solar wind electrons

is the electron/ion acoustic instability. This mode has been studied under various solar wind conditions [e.g., *Forslund*, 1970; *Gary*, 1978; *Dum et al.*, 1980]; its properties are summarized in Section 3.2.1 of *Gary* [1993]. This electrostatic mode propagates with $\omega_r < \omega_p$ and wavenumbers which scale as the inverse of the electron Debye length. Its maximum growth rate arises at $\mathbf{k} \times \mathbf{B}_o = 0$; in that direction of propagation its properties are independent of the magnetic field and the Landau resonant factors satisfy $|\zeta_p| > 2$, $|\zeta_c| \sim 0$, and $0 < |\zeta_h| < 2$.

For the dimensionless parameters of Table 1, the electron/ion acoustic instability has a much higher heat flux threshold than its whistler counterpart [e.g., Fig. 4 of *Gary*, 1978], and it does not compete with the whistler in plasmas with $T_{\|c} \sim T_p$. However, if one chooses to fix $\tilde{\beta}_{\|c}$ and raise $T_{\|c}/T_p$, the ion acoustic threshold can drop below that of the whistler. This is illustrated in Figure 3 which shows the dimensionless heat flux at threshold as a function of both $\tilde{\beta}_{\|c}$ and $T_{\|c}/T_p$. The whistler instability has the lowest heat flux threshold among all these instabilities for sufficiently large $\tilde{\beta}_{\|c}$. As this parameter decreases, its threshold increases, allowing the electron/ion acoustic instability or the Alfvén heat flux instability to assume the property of lowest threshold.

The points at which the Alfvén and ion acoustic threshold curves cross the whistler threshold curve on Figure 3 map to curves in $T_{\|c}/T_p$ versus $\tilde{\beta}_{\|c}$ space; the results are plotted as the light dashed and dotted lines in Figure 4. For a sufficiently large value of q_e/q_{max}, there is some heat flux instability which can operate over the entire parameter range illustrated here. Each curve in Figure 4 corresponds to a critical condition on $\tilde{\beta}_{\|c}$ which separates the parametric domain on which the whistler instability has the lowest threshold (right) from the domains of the electron/ion acoustic instability (upper left) and the Alfvén heat flux instability (lower left).

Thus far our linear theory has considered variations in $\tilde{\beta}_{\|c}$, $T_{\|c}/T_p$, and q_e/q_{max}, under the assumption that other dimensionless parameters are as given in Table 1. Of course, solar wind observations show that all of the electron parameters involving densities and temperatures also exhibit variations [e.g., *Phillips et al.*, 1989]. A full theoretical and observational study of each of these variations is beyond the scope of this manuscript; we here indicate the consequences of an increase in the halo temperature anisotropy, a parameter to which the whistler heat flux instability is especially sensitive.

Solar wind observations show that the halo electrons near 1 AU are not usually isotropic, but often exhibit $T_{\perp h}/T_{\|h} < 1$. This anisotropy raises the threshold heat flux of

the whistler instability, so that if this condition were incorporated into the results of Figure 3 the whistler threshold curve would move to the right and upward. The threshold of the electron/ion acoustic instability is independent of the halo anisotropy, and the Alfvén heat flux instability growth rate is almost independent of $T_{\perp h}/T_{\parallel h}$ [See Fig. 6 of *Gary et al.*, 1975]. Making the assumption that these latter two instabilities are indeed independent of the halo anisotropy, we choose $T_{\perp h}/T_{\parallel h} = 0.90$ and recalculate the whistler instability thresholds to obtain new critical conditions bounding the domains of lowest threshold. These are illustrated as the thicker dotted and dashed lines in Figure 4. This result shows that, for sufficiently low $\tilde{\beta}_{\parallel c}$, the Alfvén heat flux instability has the lowest threshold over $0.10 \leq T_{\parallel c}/T_p \leq 10.0$. We may approximate this critical condition as

$$\frac{T_{\parallel c}}{T_p} = 18\ \tilde{\beta}_{\parallel c}^{1.4} \qquad 0.05 \leq \tilde{\beta}_{\parallel c} \leq 0.50 \tag{5}$$

We have also carried out a similar calculation for the case $T_{\perp h}/T_{\parallel h} = 0.95$; this yields a critical condition for the transition from the whistler instability to the Alfvén instability in the form

$$\frac{T_{\parallel c}}{T_p} = 540\ \tilde{\beta}_{\parallel c}^{2.3} \qquad 0.04 \leq \tilde{\beta}_{\parallel c} \leq 0.15 \tag{6}$$

Interpretation

The strongest wave-particle interaction of the whistler heat flux instability is through the cyclotron resonance with the halo. This yields a pitch-angle scattering which is most effective at reducing $T_{\perp h}/T_{\parallel h}$ and the heat flux, but which affects the core temperature relatively weakly [*Gary and Feldman*, 1977]. In contrast, both the electron/ion acoustic and Alfvén heat flux instabilities have the strongest wave-particle interaction through a Landau resonance with the core (i.e., $|\zeta_c| \sim 0$); this implies that the primary roles of the enhanced fluctuating fields are to heat the core as well as to reduce the heat flux. In other words, for $\tilde{\beta}_{\parallel c}$ values less than the critical conditions shown in Figure 4, both the electron/ion acoustic and Alfvén modes should act to increase both $\tilde{\beta}_{\parallel c}$ and $T_{\parallel c}/T_p$ until the condition for excitation of the whistler heat flux instability is satisfied, at which point core heating ceases. The result of this activity would be to leave few, if any, observed conditions to the left of the appropriate curve in Figure 4. So the appropriate critical condition on $\tilde{\beta}_{\parallel c}$ should represent a lower bound for the parallel core β.

Data from Ulysses high resolution observations during January 1991, shortly after the start of the mission, are plotted as individual points in Figure 5. The electron parameters

are obtained from fits of three-dimensional observations to drifting bi-Maxwellian models for the core and halo. Here T_p is the T_{rr} or radial component of the proton temperature tensor, which is the best resolved component of that species in the Ulysses observations. For comparison the theoretical critical conditions corresponding to $T_{\perp h}/T_{\parallel h} = 0.90$ and 0.95 are also plotted. Other plots of Ulysses hourly averaged data at solar wind speeds less than 500 km/s from the early, in-ecliptic phase of the mission show similar results; for all months sampled in 1991, a line lying somewhere between Equation (5) and Equation (6) provides a good lower bound for the electron β. So we regard these equations as defining the approximate range of the lower bound on $\tilde{\beta}_{\parallel c}$ for this data set. In addition we regard the comparison shown in Figure 5 as a plausibility argument in support of our hypothesis that electron heating by the Alfvén heat flux instability imposes a lower bound on $\tilde{\beta}_{\parallel c}$ in the solar wind.

Newbury et al. [1998] report observation of enhanced whistler-like fluctuations during periods when the electron temperature is near its lower bound. This result may be taken as evidence in favor of our hypothesis (electron core heating drives the plasma toward conditions which favor growth of the whistler heat flux instability). But further research on this question seems appropriate.

Conclusions

We have used linear Vlasov dispersion theory to examine the maximum growth rates and threshold conditions of four instabilities driven by an electron heat flux with parameters similar to the average values observed near 1 AU. We confirm the well-known result that the whistler heat flux has the lowest threshold at $\tilde{\beta}_{\parallel c} \gtrsim 0.1$. However, we find that at $\tilde{\beta}_{\parallel c} \lesssim 0.1$, the mode of lowest threshold becomes either the Alfvén heat flux instability or the electron/ion acoustic instability. We note that the latter two modes are strongly Landau resonant with the core electrons, and hypothesize that, if this resonance corresponds to strong electron heating, the transition to growth of these latter instabilities represents a lower bound for $\tilde{\beta}_{\parallel c}$ in the solar wind near 1 AU. The critical condition representing the transition from the Alfvén instability to the whistler instability has been compared against data from Ulysses over 1.5 AU $< R <$ 2 AU, shows fair agreement with observations, and thereby provides a plausibility argument in support of our hypothesis.

Our conclusions and our hypothesis concerning the lower bound on $\tilde{\beta}_{\parallel c}$ should be tested through further linear theory, by fully nonlinear computer simulations and through more detailed analysis of solar wind electron and proton observations. We are unaware

of any simulation research concerning the three electromagnetic heat flux instabilities. A comparative study of these instabilities will require the use of a full electron/proton particle code, because the $T_{\|c}/T_p$ dependence of the lower bound requires that ion heating, as well as electron core heating, be allowed. Such a simulation study would also provide information about the elusive dissipation mechanism which transfers energy from the solar wind heat flux to the core electrons [*Scime et al.*, 1994b] and which cannot be attributed to the whistler heat flux instability.

For each specific choice of parameter values, as in Table 1, theory yields a specific form for the critical condition, as Equation (5) or Equation (6). However, every dimensionless plasma parameter observed by Ulysses exhibits substantial fluctuations in value, so that for any statistical solar wind data set, there should be a range of critical conditions. The observed lower bound on $\tilde{\beta}_{\|c}$ then will correspond approximately to the lowest value of this parameter over this range. The January 1991 observations should be reexamined so that a more appropriate version of Table 1 may be constructed involving both average values and ranges of likely variations for each dimensionless variable. With an improved version of Table 1, linear theory may then be revisited to construct a broader range of critical conditions, from which a more accurate lower bound may be constructed for the given data set. And, of course, it would also be useful to consider in detail larger data sets from Ulysses as well as from the relatively new ACE spacecraft.

The numerical results presented as Figures 2 through 4 are based on the parameters of Table 1. But our conclusion that there is an instability transition at sufficiently low $\tilde{\beta}_{\|c}$ and our hypothesis that this transition corresponds to a lower bound on this parameter are applicable to many collisionless plasmas which bear heat fluxes. Therefore, if our hypothesis is valid, $\tilde{\beta}_{\|c}$ should have a lower bound not only near 1 AU but throughout the solar wind and in any relatively homogeneous, collisionless plasma in which a core/halo electron distribution carries a heat flux. We recommend that Ulysses and Helios data be used to determine the lower bound on $\tilde{\beta}_{\|c}$ as a function of R, the distance from the sun, and that linear theory and computer simulations be used to predict or verify this functionality. Although *Gary et al.* [1994b] predict that the threshold of the whistler heat flux instability increases as R increases, it is necessary to determine how the thresholds of the other heat flux instabilities respond to changes in R before one can predict how the lower bound on $\tilde{\beta}_{\|c}$ may respond.

Although we have found a constraint on $\tilde{\beta}_{\|c}$ which is similar to Equation (3), our

research has not yet yielded a bound on an electron/proton temperature ratio similar to Equation (4). If such a constraint is due to wave-particle scattering, it is likely that it would be due to an instability which attains a large growth rate and heats electrons as an electron/proton temperature ratio decreases. However, with the exception of the whistler, all the heat flux instabilities studied here have growth rates which increase with increasing $T_{\|c}/T_p$. Thus heat flux instabilities appear unlikely to account for the observed bound corresponding to Equation (4).

Two other sources of free energy in the solar wind are the frequently observed proton beams and relative streaming between the proton and alpha particle components which can give rise to a variety of ion/ion instabilities [*Montgomery et al.*, 1975, 1976; *Gary*, 1978] which may contribute to Equation (4). The primary action of wave-particle scattering by these modes should be to reduce the relative streaming of the ion components, thereby reducing the apparent proton temperature. However, like the heat flux instabilities, ion/ion instabilities have growth rates which are either independent of T_e/T_p or which increase with this parameter, and are not likely to operate at $T_e << T_p$, where Equation (4) is observed. To test this possibility, observations at relatively low values of electron/proton temperature ratios should be examined for a correlation with proton beams or a relatively large value of the proton/alpha relative streaming speed. Such a study would also provide additional information about the observed values of T_p which we here have assumed to have been obtained from thermal, Maxwellian-like distributions.

Coulomb collisions between electrons and ions, although rare in the solar wind, act to reduce the temperature difference between the two species, and may contribute to a lower bound on an electron/proton temperature ratio. However, *Newbury et al.* [1998] found that plasma densities are relatively low for those points which lie near the bound represented by Equation (1), reducing the likelihood that the effect is due to collisions.

Collisionless shocks typically heat ions more strongly than electrons [e.g., *Thomsen et al.*, 1985]. Equation (4) may represent the maximum heating of protons by such shocks, under the assumption that Coulomb collisions and other processes subsequently act to increase T_e/T_p. To test this possibility, solar wind observations at relatively low values of electron/proton temperature ratios should be examined for a correlation with shock passages.

Appendix: Definitions

We use the subscripts $\|$ and $\perp$ to denote directions relative to $\mathbf{B}_o$, the background

magnetic field. The average drift velocity of the jth component parallel to $\mathbf{B}_o$ is denoted by $\mathbf{v}_{oj}$, and the relative core/halo average drift velocity is $\mathbf{v}_o = \mathbf{v}_{oc} - \mathbf{v}_{oh}$. We define the parallel β of the jth component or species to be $\beta_{\|j} \equiv 8\pi n_j k_B T_{\|j}/B_o^2$. A useful dimensionless measure of the temperature of the jth component is $\tilde{\beta}_{\|j} \equiv 8\pi n_p k_B T_{\|j}/B_o^2$. We also define the cyclotron frequency of the jth species, $\Omega_j \equiv e_j B_o/m_j c$, the thermal speed of the jth species or component, $v_j \equiv \sqrt{k_B T_{\|j}/m_j}$, the plasma frequency of the jth species, $\omega_j \equiv \sqrt{4\pi n_j e_j^2/m_j}$, and θ, the angle between the wavevector $\mathbf{k}$ and $\mathbf{B}_o$. If both the halo and core are described in terms of drifting bi-Maxwellian distributions, the heat flux is

$$q_e = \frac{m_e}{2} \sum_{j=c,h} n_j v_{oj} \left[\left(3 + 2\frac{T_{\perp j}}{T_{\|j}} \right) v_j^2 + v_{oj}^2 \right]$$

We define the heat flux normalization factor as $q_{max} \equiv 3 m_e n_e v_c^3/2$.

The character of the wave-particle interaction between a mode and a particle component or species is determined by the resonant factors which appear as arguments of the plasma dispersion function in the linear Vlasov equation [e.g., *Gary*, 1993]. The Landau resonant factor is

$$\zeta_j \equiv \frac{\omega - \mathbf{k} \cdot \mathbf{v}_{oj}}{\sqrt{2} k_\| v_j}$$

and the cyclotron resonant factor is

$$\zeta_j^\pm \equiv \frac{\omega - \mathbf{k} \cdot \mathbf{v}_{oj} \pm \Omega_j}{\sqrt{2} k_\| v_j}$$

Small or intermediate values of these factors ($|\zeta| < 3$) correspond to a resonant wave-particle interaction, whereas relatively large values such as $|\zeta| > 5$ imply that the corresponding wave-particle interaction is nonresonant or fluid-like.

If we fix all plasma physical dimensionless parameters, and solve the linear Vlasov dispersion equation for all values of wavenumber k and propagation angle θ, we denote the resulting maximum growth rate as γ_m. If we perform this same exercise many times for a wide domain of q_e/q_{max}, and it turns out that a particular instability yields a relative maximum value of the maximum growth rate on this domain, we denote this by the symbol γ_{mm} and term this the "overall maximum growth rate." The whistler and magnetosonic heat flux instabilities exhibit overall maximum growth rates (see Fig. 8.10 of *Gary* [1993] and Fig. 3 of *Gary et al.* [1975a]), whereas the Alfvén heat flux and electron/ion acoustic instabilities have dimensionless maximum growth rates which monotonically increase with increasing q_e/q_{max} (see Fig. 3 of *Gary et al.* [1975a] and Fig. 3.6 of *Gary* [1993]).

Acknowledgments. We acknowledge useful discussions with Bill Feldman, Jack Gosling, Pete Riley, and especially Ruth Skoug. The Los Alamos portion of this work was performed under the auspices of the U.S. Department of Energy (DOE) and was supported in part by the DOE Office of Basic Energy Sciences, Division of Engineering and Geosciences, the Laboratory Directed Research and Development program at Los Alamos, and the Institute for Geophysics and Planetary Physics at Los Alamos.

References

Anderson, B. J., and S. A. Fuselier, Magnetic pulsations from 0.1 to 4.0 Hz and associated plasma properties in the Earth's subsolar magnetosheath and depletion layer, *J. Geophys. Res.*, **98**, 1461, 1993.

Anderson, B. J., S. A. Fuselier, S. P. Gary, and R. E. Denton, Magnetic spectral signatures in the Earth's magnetosheath and plasma depletion layer, *J. Geophys. Res.*, **99**, 5877, 1994.

Bame, S. J., D. J. McComas, B. L. Barraclough, J. L. Phillips, K. J. Sofaly, J. C. Chavez, B. E. Goldstein, and R. K. Sakurai, The Ulysses solar wind plasma experiment, *Astron. and Astrophys., suppl. Ser.*, **92**, 221, 1992.

Dum, C. T., E. Marsch, and W. Pilipp, Determination of wave growth from measured distribution functions and transport theory, *J. Plasma Phys.*, **23**, 91, 1980.

Feldman, W. C., J. R. Asbridge, S. J. Bame, and M. D. Montgomery, Interpenetrating solar wind streams, *Revs. Geophys.*, **4**, 715, 1974.

Feldman, W. C., J. R. Asbridge, S. J. Bame, M. D. Montgomery, and S. P. Gary, Solar wind electrons, *J. Geophys. Res.*, **80**, 4181, 1975.

Forslund, D. W., Instabilities associated with heat conduction in the solar wind and their consequences, *J. Geophys. Res.*, **75**, 17, 1970.

Fuselier, S. A., B. J. Anderson, S. P. Gary, and R. E. Denton, Inverse correlations between the ion temperature anisotropy and plasma beta in the Earth's quasi-parallel magnetosheath, *J. Geophys. Res.*, **99**, 14,931, 1994.

Gary, S. P., Ion-acoustic-like instabilities in the solar wind, *J. Geophys. Res.*, **83**, 2504, 1978.

Gary, S. P., Theory of Space Plasma Microinstabilities, Cambridge University Press, Cambridge, 1993.

Gary, S. P., and W. C. Feldman, Solar wind heat flux regulation by the whistler instability, *J. Geophys. Res.*, **82**, 1087, 1977.

Gary, S. P., W. C. Feldman, D. W. Forslund, and M. D. Montgomery, Electron heat flux instabilities in the solar wind, *Geophys. Res. Lett.*, **2**, 79, 1975a.

Gary, S. P., W. C. Feldman, D. W. Forslund, and M. D. Montgomery, Heat flux instabilities in the solar wind, *J. Geophys. Res.*, **80**, 4197, 1975b.

Gary, S. P., B. J. Anderson, R. E. Denton, S. A. Fuselier, and M. E. McKean, A limited closure relation for anisotropic plasmas from the Earth's magnetosheath, *Phys. Plasmas*, **1**, 1676, 1994a.

Gary, S. P., E. E. Scime, J. L. Phillips, and W. C. Feldman, The whistler heat flux instability: Threshold conditions in the solar wind, *J. Geophys. Res.*, **99**, 23,391, 1994b.

Gary, S. P., M. F. Thomsen, L. Yin, and D. Winske, Electromagnetic proton cyclotron instability: Interactions with magnetospheric protons, *J. Geophys. Res.*, **100**, 21,961, 1995.

Maksimovic, M., S. Hoang, N. Meyer-Vernet, M. Moncuquet, J.-L Bougeret, J. L. Phillips, and P. Canu, Solar wind electron parameters from quasi-thermal noise spectroscopy and comparison with other measurements on Ulysses, *J. Geophys. Res.*, **100**, 19,881, 1995.

Marsch, E., Kinetic physics of the solar wind plasma, in *Physics of the Inner Heliosphere II, Particles, Waves and Turbulence*, edited by R. Schwenn and E. Marsch, p. 135, Springer-Verlag, New York, 1991.

Montgomery, M. D., S. P. Gary, and D. W. Forslund, Electromagnetic ion-beam instabilities in the solar wind, *Phys. Rev. Lett.*, **35**, 667, 1975.

Montgomery, M. D., S. P. Gary, W. C. Feldman, and D. W. Forslund, Electromagnetic instabilities driven by unequal proton beams in the solar wind, *J. Geophys. Res.*, **81**, 2743, 1976.

Newbury, J. A., C. T. Russell, and J. L. Phillips, Electron temperature in the ambient solar wind: Typical properties and a lower bound at 1 AU, *J. Geophys. Res.*, **103**, xxxx, 1998.

Phillips, J. L., J. T. Gosling, D. J. McComas, S. J. Bame, S. P. Gary, and E. J. Smith, Anisotropic thermal electron distributions in the solar wind, *J. Geophys. Res.*, **94**, 6563, 1989.

Phillips, J. L., S. J. Bame, S. P. Gary, J. T. Gosling, E. E. Scime, and R. J. Forsyth, Radial and meridional trends in solar wind thermal electron temperature and anisotropy: Ulysses, *Space Science Reviews*, **72**, 109, 1995.

Richardson, I. G., C. J. Farrugia, and H. V. Cane, A statistical study of the behavior of the electron temperature in ejecta, *J. Geophys. Res.*, **102**, 4691, 1997.

Scime, E. E., J. L. Phillips, and S. J. Bame, Effects of spacecraft potential on three-dimensional electron measurements in the solar wind, *J. Geophys. Res.*, **99**, 14,769, 1994a.

Scime, E. E., S. J. Bame, W. C. Feldman, S. P. Gary, and J. L. Phillips, Regulation of the solar wind electron heat flux from 1 to 5 AU: Ulysses observations, *J. Geophys. Res.*, **99**, 23,401, 1994b.

Thomsen, M. F., J. T. Gosling, S. J. Bame, and M. M. Mellott, Ion and electron heating at collisionless shocks near the critical Mach number, *J. Geophys. Res.*, **90**, 137, 1985.

S. P. Gary, M.S. D466, Los Alamos National Laboratory, Los Alamos, NM 87545. (e-mail: pgary@lanl.gov; url: http://nis-www.lanl.gov/~pgary/).

J. A. Newbury, Institute of Geophysics and Planetary Physics, University of California, Los Angeles, Los Angeles, CA 90095-1567. (e-mail: newbury@igpp.ucla.edu)

B. E. Goldstein, MS 169-506, Jet Propulsion Laboratory, 4800 Oak Grove Drive, Pasadena, CA 91109. (e-mail: bgoldstein@jplsp.jpl.nasa.gov)

Figure Captions

Figure 1. Observational results: Electron halo temperature anisotropies as functions of the core parallel β from Ulysses high resolution observations during January 1991. Here and in Figure 5 electron parameters are obtained from fits to three-dimensional velocity distributions using drifting bi-Maxwellian models for the core and halo.

Figure 2. Linear Vlasov theory results: The maximum growth rate for three heat flux instabilities as a function of the dimensionless electron heat flux for three different values of $\tilde{\beta}_{\|c}$ with all other dimensionless parameters as given in Table 1. The numbers labeling each curve represent the corresponding values of $\tilde{\beta}_{\|c}$. The solid lines represent the magnetosonic heat flux instability; the regular dashed lines represent the Alfvén heat flux instability; and the long dash-short dashed lines represent the whistler heat flux instability. At $\tilde{\beta}_{\|c} = 0.05$, the magnetosonic heat flux instability has a very weak growth rate such that $\gamma_m < 3 \times 10^{-5}\Omega_p$.

Figure 3. Linear Vlasov theory results: The dimensionless heat flux at instability threshold of $\gamma_m = 10^{-3}\Omega_p$ for three different instabilities as a function of $\tilde{\beta}_{\|c}$. All di-

mensionless parameters are as given in Table 1 except for the values of $T_{\|c}/T_p$ and the fixed value $T_{\|h}/T_{\|c} = 6$. The corresponding values of $T_{\|c}/T_p$ are indicated; the threshold condition of the whistler heat flux instability is independent of this temperature ratio. The dotted lines represent the electron/ion acoustic instability; the regular dashed lines represent the Alfvén heat flux instability; and the long dash-short dashed line represents the whistler heat flux instability.

Figure 4. Linear Vlasov theory results: The domains of lowest threshold for three instabilities in $T_{\|c}/T_p$ versus $\tilde{\beta}_{\|c}$ space. The dashed lines represent the transition from the Alfvén heat flux instability (left) to the whistler heat flux instability (right); the dotted lines represent the transition from the domain of the electron/ion acoustic instability (upper left) to the whistler heat flux instability (lower right). The light dashed and light dotted lines correspond to the conditions of Table 1 (e.g., Figure 3), whereas the heavier dashed and dotted lines correspond to the conditions of Table 1 except that $T_{\perp h}/T_{\|h} = 0.90$.

Figure 5. Observational results: Core electron/proton temperature ratios as functions of the parallel core β from Ulysses high resolution observations during January 1991. The solid and dashed lines represents the theoretical conditions, Equation (5) and Equation (6), as derived under the conditions of Table 1 with $T_{\perp h}/T_{\|h} = 0.90$ and $T_{\perp h}/T_{\|h} = 0.95$, respectively.

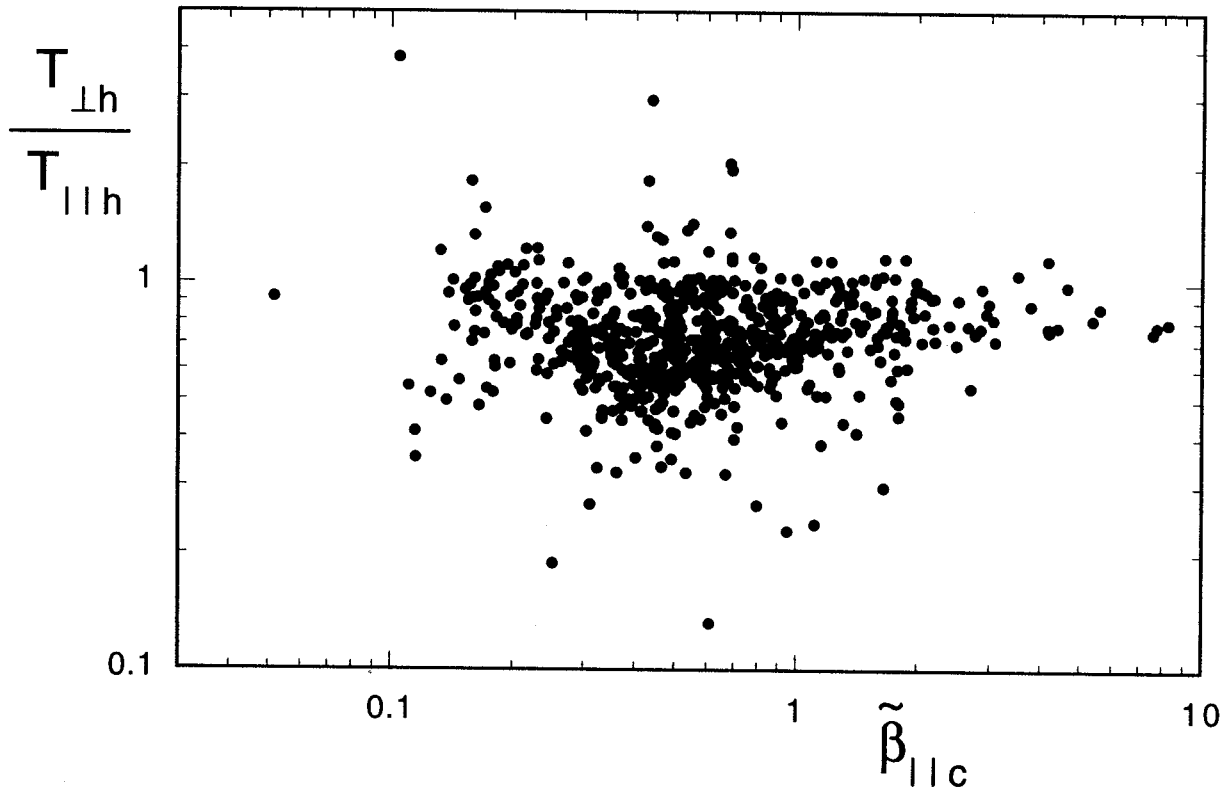

Figure 1

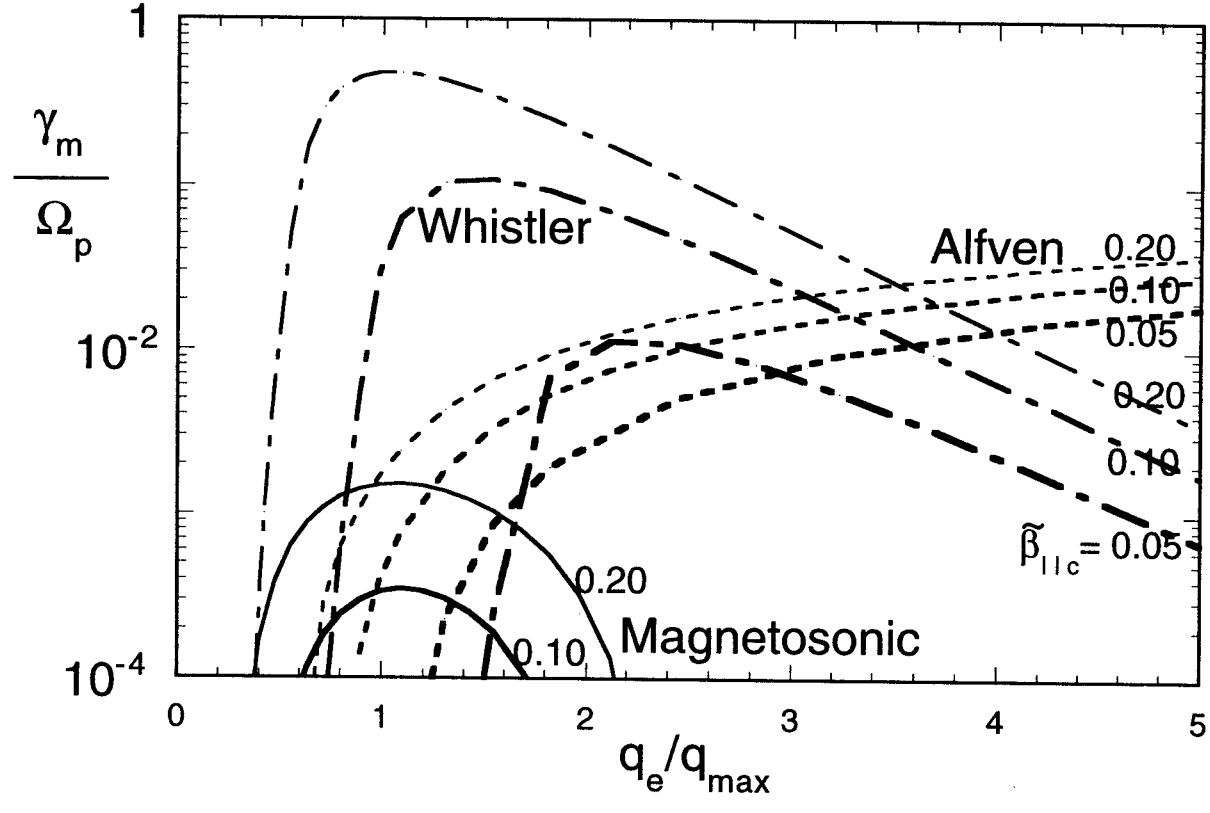
1
$\frac{\gamma_m}{\Omega_p}$
10^{-2}
10^{-4}
Whistler
Alfven
0.20
0.10
0.05
0.20
0.10
$\tilde{\beta}_{\parallel c}$= 0.05
0.20
0.10
Magnetosonic
0
1
2
3
4
5
q_e/q_{max}

Figure 2

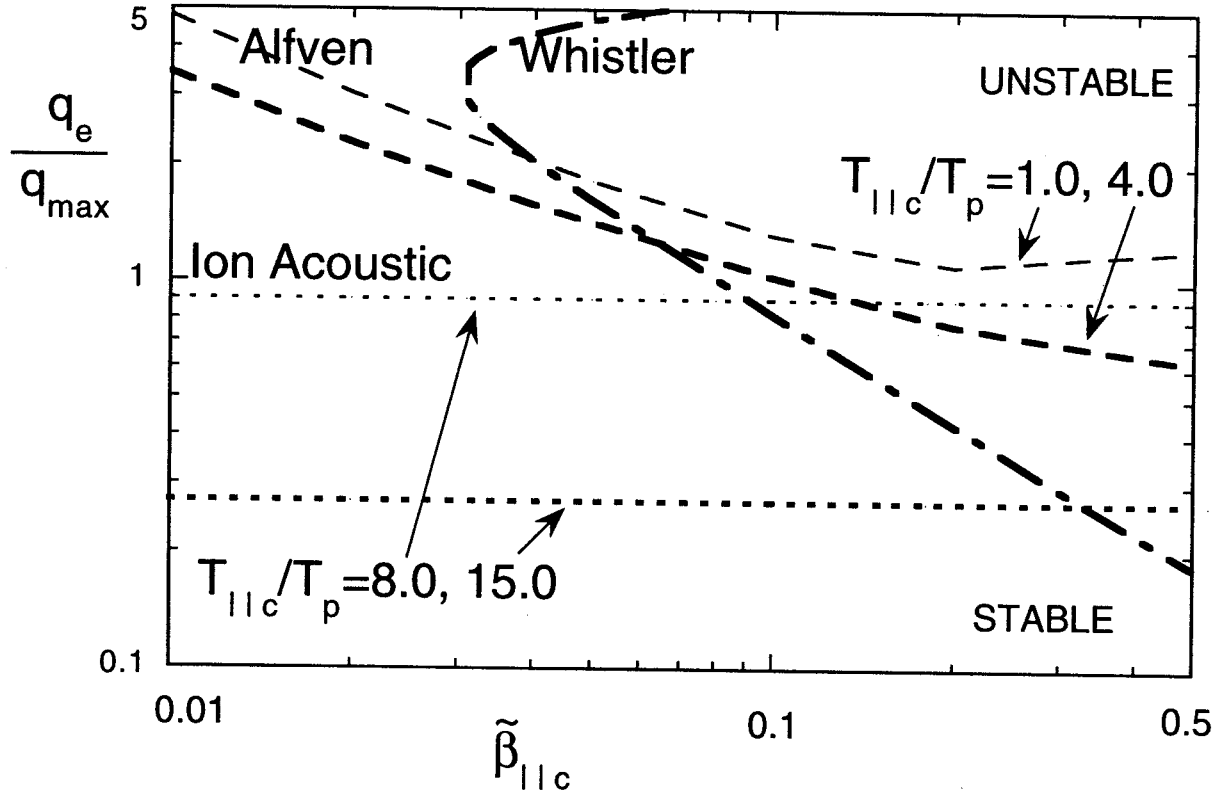
5
1
0.1
$\frac{q_e}{q_{max}}$
Alfven
Whistler
UNSTABLE
$T_{\|c}/T_p$=1.0, 4.0
Ion Acoustic
$T_{\|c}/T_p$=8.0, 15.0
STABLE
0.01
0.1
0.5
$\tilde{\beta}_{\|c}$

Figure 3

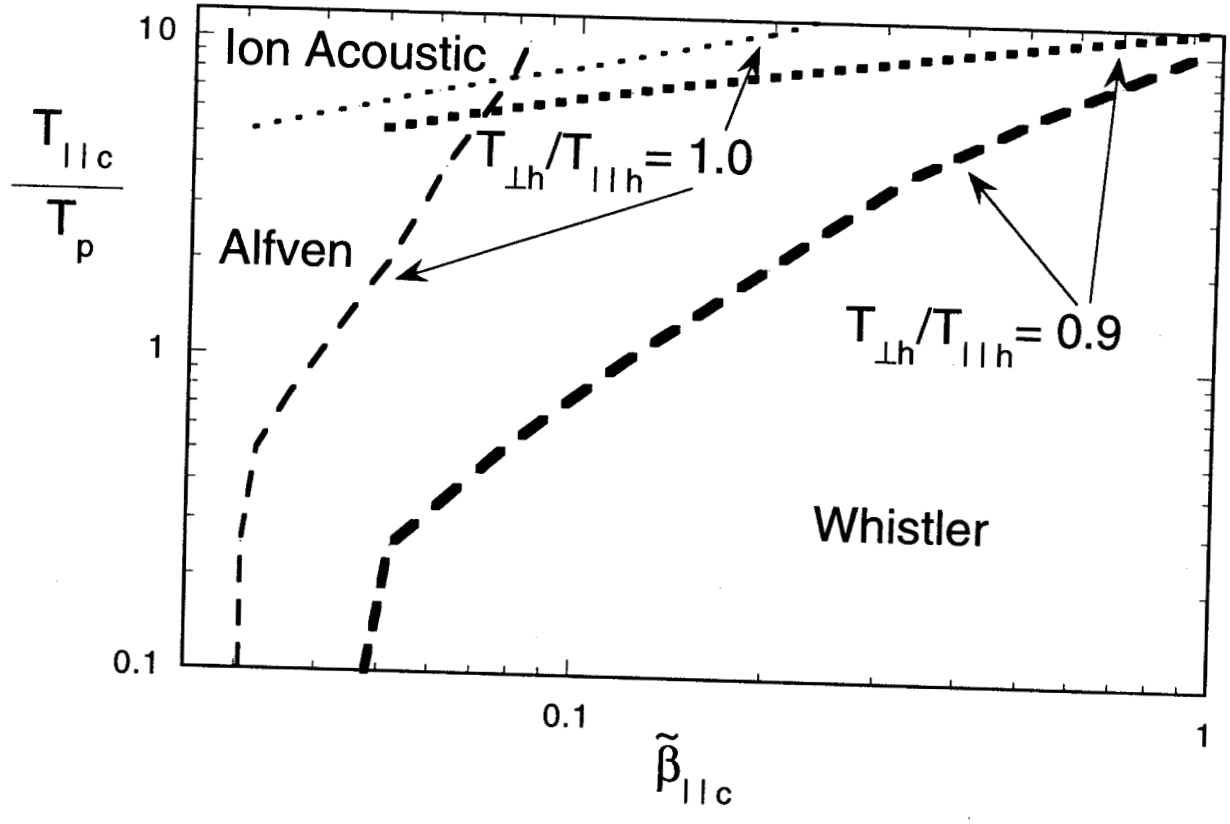
10
1
0.1
0.1
1
$\frac{T_{\|c}}{T_p}$
$\tilde{\beta}_{\|c}$
Ion Acoustic
$T_{\perp h}/T_{\|h}$= 1.0
Alfven
$T_{\perp h}/T_{\|h}$= 0.9
Whistler

Figure 4

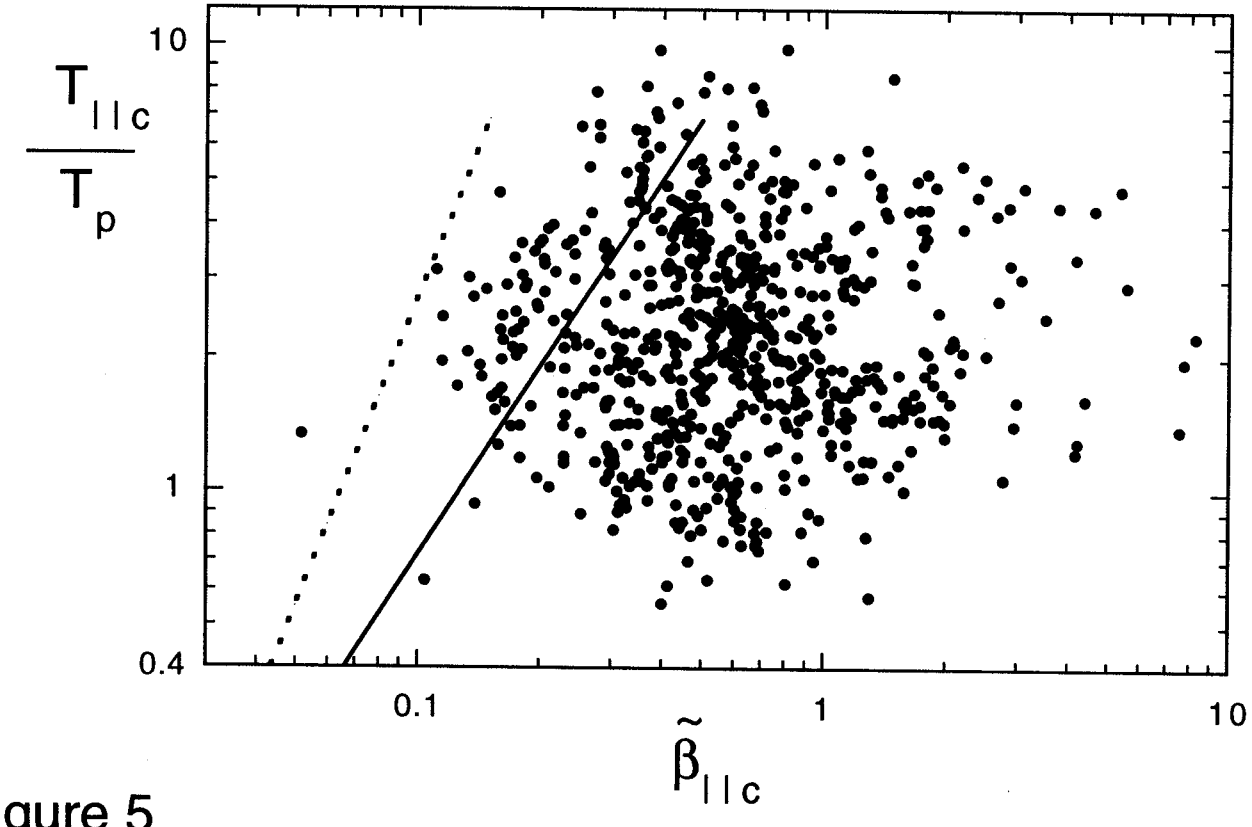

Figure 5